

# Diffractive dissociation of gluons into heavy quark-antiquark pairs in proton-proton collisions

Marta Łuszczak,<sup>1,\*</sup> Wolfgang Schäfer,<sup>2,†</sup> and Antoni Szczurek<sup>2,1,‡</sup>

<sup>1</sup>*Institute of Physics, University of Rzeszów, PL-35-959 Rzeszów, Poland*

<sup>2</sup>*Institute of Nuclear Physics PAN, PL-31-342 Kraków, Poland*

(Dated: June 28, 2018)

## Abstract

We discuss diffractive dissociation of gluons into heavy quark pairs. The particular mechanism is similar to the diffractive dissociation of virtual photons into quarks, which drives diffractive deep inelastic production of charm in the low-mass diffraction, or large  $\beta$ -region. There, it can be understood, with some reservations, in terms of a valence heavy quark content of the Pomeron. The amplitude for the  $gp \rightarrow Q\bar{Q}p$  is derived in the impact parameter and momentum space. The cross section for single diffractive  $pp \rightarrow Q\bar{Q}pX$  is calculated as a convolution of the elementary cross section and gluon distribution in the proton. Integrated cross section and the differential distributions in e.g. transverse momentum and rapidity of the charm and bottom quark and antiquark, as well as the quark-antiquark invariant mass are calculated for the nominal LHC energy for different unintegrated gluon distributions from the literature. The ratio of the bottom-to-charm cross sections are shown and discussed as a function of several kinematical variables.

arXiv:1305.4727v1 [hep-ph] 21 May 2013

---

\*Electronic address: [luszczak@univ.rzeszow.pl](mailto:luszczak@univ.rzeszow.pl)

†Electronic address: [Wolfgang.Schafer@ifj.edu.pl](mailto:Wolfgang.Schafer@ifj.edu.pl)

‡Electronic address: [Antoni.Szczurek@ifj.edu.pl](mailto:Antoni.Szczurek@ifj.edu.pl)

## I. INTRODUCTION

Hard diffractive production is a special class of diffractive processes. It is characterized by the production of massive objects ( $W^\pm$ ,  $Z^0$ , Higgs boson, pairs of heavy quark - heavy antiquark) or objects with large transverse momenta (jets, dijets) and one (single diffractive process) or two (central diffractive process) rapidity gaps between proton(s) and the centrally produced massive system. The cross section for these processes is often calculated in terms of hard matrix elements for a given process and so-called diffractive parton distributions, for a review, see e.g. [1]. The latter are often calculated, following a suggestion of Ingelman and Schlein [2], in a purely phenomenological approach in terms of parton distributions in the pomeron and a Regge-theory motivated flux of Pomerons. It is understood that such a factorization in hadron-hadron collisions must be broken [3]. To quantify absorptive corrections one often uses a global gap survival factor. For recent discussions on models of the gap survival, see eg. [4, 5].

Diffractive production of heavy quarks was previously discussed within the Ingelman-Schlein model in Refs.[6–9] and proposed as a probe of the hard substructure of the Pomeron.

In this paper we wish to discuss a specific mechanism for the diffractive production of heavy quark – antiquark pairs in proton-proton collisions in a “microscopic approach” which does not use the assumptions of Regge factorization, and in which the QCD Pomeron is rather modelled by exchange of a gluon ladder related to the unintegrated gluon distribution in the proton.

The mechanism we propose is based on the partonic subprocess  $gp \rightarrow Q\bar{Q}p$  – the diffractive dissociation of a gluon into a heavy quark pair. At the first sight it may be surprising that diffraction of a colored parton is a meaningful thing to consider, but it turns out that the forward amplitude for the  $gp \rightarrow Q\bar{Q}p$  is well behaved and perturbatively calculable without introducing new soft parameters.

Our mechanism has much in common – in fact the both amplitudes turn out to be proportional to each other– with the diffractive dissociation of a virtual photon into quarks  $\gamma^*p \rightarrow Q\bar{Q}p$  through two-gluon exchange first introduced in [10]. Although there are many caveats, e.g. considering the Regge factorization, with certain reservations the results of [10] can be formulated in terms of a valence quark structure of the Pomeron, see for example the discussions in [11–13]. The case of diffractive deep inelastic production of open charm was studied in this approach in detail first in [14].

In the usual treatment of hard diffraction, heavy quarks are generated from gluons in the Pomeron and a valence-like heavy quark contribution is not present. In this sense the mechanism discussed here is complementary to existing approaches, although eventually we intend that the Ingelman-Schlein mechanism be superseded also by a microscopic model for the glue in the Pomeron.

From the experimental point of view there is a clear-cut kinematical distinction between the heavy quark production discussed of Fig.1 here and the standard approach: our  $Q\bar{Q}$  pairs are produced in the Pomeron fragmentation region, close to the rapidity gap, whereas gluon-fusion generated heavy quarks populate a large part of the phase space taken up by the diffractively produced system and will generally give a tiny contribution in the Pomeron fragmentation region, unless there are a lot of hard gluons in

the Pomeron.

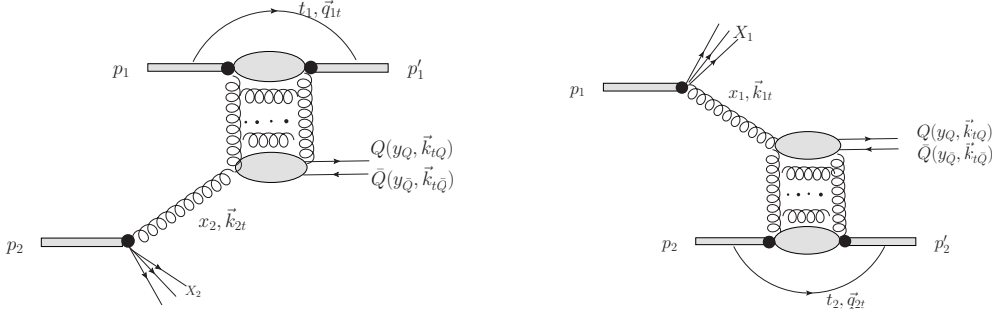


FIG. 1: The mechanism of gluon dissociation into  $Q\bar{Q}$  via exchange of gluonic ladder in proton-proton collisions.

In fact we are not the first to consider this mechanism of hard diffraction in hadronic interactions: the same partonic amplitudes were calculated previously in [15, 16], although in an approximation in which gluon transverse momenta in the Pomeron are integrated out. Our results appear to be different from those presented in [15, 16]. We also mention that related, but different microscopic mechanisms are discussed in [17]), however only a Feynman  $x_F$  distribution was presented there.

In the present paper we wish to present our amplitude for the  $gp \rightarrow Q\bar{Q}p$  (sub)process. We wish to calculate also integrated and differential cross section for the  $pp \rightarrow Q\bar{Q}pX$  single-diffractive processes at the LHC. We will compare the cross section for the single diffractive process of charm and bottom. Furthermore we will show some differential distributions, e.g. in rapidity and transverse momentum for LHC energy. Conclusions and outlook close our paper.

## II. DIFFRACTIVE AMPLITUDE FOR $gp \rightarrow Q\bar{Q}p$

A salient feature of high-energy interactions is that partons move along straight line trajectories, and impact parameters are conserved during the interaction with the target, which is mediated by the  $t$ -channel gluon exchanges.

The amplitude for the diffractive process  $gN \rightarrow Q\bar{Q}N$  can be written in impact-parameter space, where the impact parameters of gluon, quark and antiquark are  $\mathbf{b}, \mathbf{b}_+, \mathbf{b}_-$ , respectively:

$$\mathcal{A}_D(g_{\lambda_g}^a N \rightarrow Q_{\lambda} \bar{Q}_{\bar{\lambda}} N) = \int [\mathcal{D}\mathbf{b}] \exp[-i\mathbf{p}_+ \mathbf{b}_+ - i\mathbf{p}_- \mathbf{b}_-] \langle N | \mathcal{M}^a(\mathbf{b}_+, \mathbf{b}_-, \mathbf{b}) | N \rangle \psi_{\lambda, \bar{\lambda}}^{\lambda_g}(z, \mathbf{b}_+ - \mathbf{b}_-), \quad (1)$$

The integration over impact parameters explicitly reads

$$[\mathcal{D}\mathbf{b}] = d^2\mathbf{b}_+ d^2\mathbf{b}_- d^2\mathbf{b} \delta^{(2)}(\mathbf{b} - z\mathbf{b}_+ - (1-z)\mathbf{b}_-). \quad (2)$$

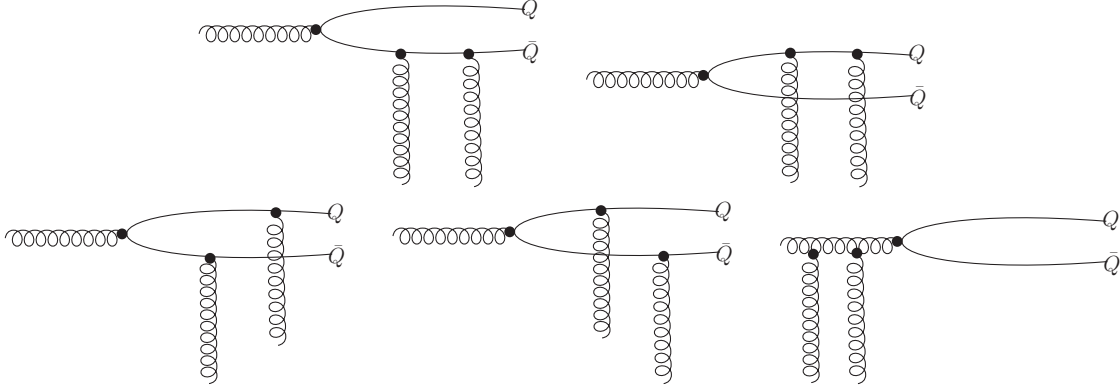


FIG. 2: Diagrams contributing to the diffractive gluon dissociation into  $Q\bar{Q}$ . The two gluons in the  $t$ -channel are in the color singlet state.

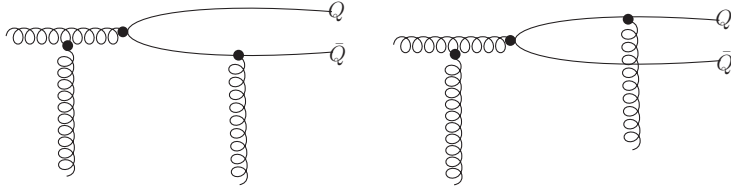


FIG. 3: Diagrams which do not contribute to the gluon dissociation into  $Q\bar{Q}$  in the high-energy limit.

Quark and antiquark share the lightcone-momentum of the incoming gluon in fractions  $z, 1 - z$ , and have the transverse momenta  $\mathbf{p}_+, \mathbf{p}_-$ , respectively. The transition  $g_{\lambda_g} \rightarrow Q_\lambda \bar{Q}_{\bar{\lambda}}$  is described by the lightcone wave-function  $\psi_{\lambda, \bar{\lambda}}^{\lambda_g}$ . The interaction of partons with the target is encoded in the operator [18]

$$\mathcal{M}^a(\mathbf{b}_+, \mathbf{b}_-, \mathbf{b}) = \left[ S(\mathbf{b}_+) t^a S^\dagger(\mathbf{b}_-) - S(\mathbf{b}) t^a S^\dagger(\mathbf{b}) \right]. \quad (3)$$

Here the quark-proton  $S$ -matrix  $S(\mathbf{b}_+)$  is written in terms of the gluon-exchange eikonal  $\hat{\chi} = \chi^a t^a$ , as

$$S(\mathbf{b}_+) = 1 + i\hat{\chi}(\mathbf{b}_+) - \frac{1}{2}\hat{\chi}^2(\mathbf{b}_+), \quad (4)$$

the antiquark interacts with the complex-conjugate  $S$ -matrix  $S^\dagger(\mathbf{b}_-)$ , and a gluon interacts in the same fashion as a pointlike color-octet  $Q\bar{Q}$  pair and its scattering is described by  $S(\mathbf{b}) t^a S^\dagger(\mathbf{b})$  [18].

As we are interested in a diffractive process, with no color-transfer to the target, in the evaluation of the nucleon-matrix element  $\langle N | \mathcal{M}^a(\mathbf{b}_+, \mathbf{b}_-, \mathbf{b}) | N \rangle$ , only the terms of quadratic order in the eikonal will contribute. Indeed, they correspond to the coupling of two gluons in the color-singlet state to the nucleon:

$$\langle N | \chi^a(\mathbf{b}_+) \chi^b(\mathbf{b}_-) | N \rangle = \delta^{ab} \chi^{(2)}(\mathbf{b}_+, \mathbf{b}_-), \quad (5)$$

which we parametrize as

$$C_F \cdot \chi^{(2)}(\mathbf{b}_+, \mathbf{b}_-) = \int \frac{d^2\mathbf{q}}{(2\pi)^2} \frac{d^2\boldsymbol{\kappa}}{(2\pi)^2} f(x, \frac{\mathbf{q}}{2} + \boldsymbol{\kappa}, \frac{\mathbf{q}}{2} - \boldsymbol{\kappa}) \exp[i\frac{\mathbf{q}}{2}(\mathbf{b}_+ + \mathbf{b}_-)] \exp[i\boldsymbol{\kappa}(\mathbf{b}_+ - \mathbf{b}_-)]. \quad (6)$$

Here the function  $f$  is a generalized two-gluon density matrix, including gluon propagators, and off-diagonal in transverse momenta. It takes the form

$$f(x, \boldsymbol{\kappa}_1, \boldsymbol{\kappa}_2) = \frac{(2\pi)^3}{N_c} \cdot \frac{\alpha_S \mathcal{F}(x, \boldsymbol{\kappa}_1, \boldsymbol{\kappa}_2)}{\boldsymbol{\kappa}_1^2 \boldsymbol{\kappa}_2^2}, \quad (7)$$

where in turn  $\mathcal{F}$ , at large  $\boldsymbol{\kappa}^2$  is related to the familiar unintegrated gluon structure function as

$$\mathcal{F}(x, \boldsymbol{\kappa}, -\boldsymbol{\kappa}) = \frac{\partial[xg(x, \boldsymbol{\kappa}^2)]}{\partial \log(\boldsymbol{\kappa}^2)}. \quad (8)$$

The full  $f$  is often parametrized as

$$f(x, \frac{\mathbf{q}}{2} + \boldsymbol{\kappa}, \frac{\mathbf{q}}{2} - \boldsymbol{\kappa}) = \frac{(2\pi)^3}{N_c} \frac{\alpha_S}{\boldsymbol{\kappa}^4} \frac{\partial[xg(x, \boldsymbol{\kappa}^2)]}{\partial \log(\boldsymbol{\kappa}^2)} \exp[-\frac{1}{2}B_D \mathbf{q}^2], \quad (9)$$

where the diffractive slope  $B_D$  is a nonperturbative quantity that takes care of the effective size of the target. In accord with Regge-phenomenology, it has an  $x$ -dependent piece,  $B_D = B_0 + \alpha'_{\mathbf{P}} \log(x_0/x)$ . In our numerical calculations, we use an educated guess for the diffractive slope [19]:  $B_0 = 4.0 \text{ GeV}^{-2}$ ,  $\alpha'_{\mathbf{P}} = 0.164$ .

We then obtain:

$$\langle N | \mathcal{M}^a(\mathbf{b}_+, \mathbf{b}_-, \mathbf{b}) | N \rangle = t^a \left\{ \frac{1}{2N_c C_F} \Gamma^{(2)}(\mathbf{b}_+, \mathbf{b}_-) - \frac{N_c}{2C_F} \bar{\Gamma}^{(2)}(\mathbf{b}_+, \mathbf{b}_-) \right\}, \quad (10)$$

where

$$\begin{aligned} \Gamma^{(2)}(\mathbf{b}_+, \mathbf{b}_-) &= \frac{C_F}{2} \cdot \left[ \chi^{(2)}(\mathbf{b}_+, \mathbf{b}_+) + \chi^{(2)}(\mathbf{b}_-, \mathbf{b}_-) - \chi^{(2)}(\mathbf{b}_+, \mathbf{b}_-) - \chi^{(2)}(\mathbf{b}_-, \mathbf{b}_+) \right], \\ \bar{\Gamma}^{(2)}(\mathbf{b}_+, \mathbf{b}_-) &= \frac{C_F}{2} \cdot \left[ \chi^{(2)}(\mathbf{b}_+, \mathbf{b}_+) + \chi^{(2)}(\mathbf{b}_-, \mathbf{b}_-) - 2\chi^{(2)}(\mathbf{b}, \mathbf{b}) \right]. \end{aligned} \quad (11)$$

Here the profile function  $\Gamma^{(2)}(\mathbf{b}_+, \mathbf{b}_-)$  is related to the familiar color-dipole cross section through the relation

$$\sigma(\mathbf{r}) = 2 \int d^2\mathbf{B} \Gamma^{(2)}(\mathbf{B} + \frac{\mathbf{r}}{2}, \mathbf{B} - \frac{\mathbf{r}}{2}). \quad (12)$$

Following [20], we can write the relevant profile functions in terms of the off-diagonal

gluon density as:

$$\begin{aligned}
\Gamma^{(2)}(\mathbf{b}_+, \mathbf{b}_-) &= \int \frac{d^2\mathbf{q}}{(2\pi)^2} \frac{d^2\boldsymbol{\kappa}}{(2\pi)^2} f(x, \frac{\mathbf{q}}{2} + \boldsymbol{\kappa}, \frac{\mathbf{q}}{2} - \boldsymbol{\kappa}) \exp[i\frac{\mathbf{q}}{2}(\mathbf{b}_+ + \mathbf{b}_-)] , \\
&\times \left\{ \exp[i\frac{\mathbf{q}}{2}(\mathbf{b}_+ - \mathbf{b}_-)] + \exp[-i\frac{\mathbf{q}}{2}(\mathbf{b}_+ - \mathbf{b}_-)] \right. \\
&\quad \left. - \exp[i\boldsymbol{\kappa}(\mathbf{b}_+ - \mathbf{b}_-)] - \exp[-i\boldsymbol{\kappa}(\mathbf{b}_+ - \mathbf{b}_-)] \right\} , \\
\bar{\Gamma}^{(2)}(\mathbf{b}_+, \mathbf{b}_-) &= \int \frac{d^2\mathbf{q}}{(2\pi)^2} \frac{d^2\boldsymbol{\kappa}}{(2\pi)^2} f(x, \frac{\mathbf{q}}{2} + \boldsymbol{\kappa}, \frac{\mathbf{q}}{2} - \boldsymbol{\kappa}) \left[ \exp[i\mathbf{q}\mathbf{b}_+] + \exp[i\mathbf{q}\mathbf{b}_-] - 2\exp[i\mathbf{q}\mathbf{b}] \right] .
\end{aligned} \tag{13}$$

We now introduce the usual parametrization of transverse momenta: the decorrelation momentum of jets (or momentum transfer to the proton)  $\boldsymbol{\Delta} = \mathbf{p}_+ + \mathbf{p}_-$  and the light-cone relative transverse momentum  $\mathbf{k} = (1-z)\mathbf{p}_+ - z\mathbf{p}_-$ , which is conjugate to the dipole size  $\mathbf{r} = \mathbf{b}_+ - \mathbf{b}_-$ . We then notice, that

$$[\mathcal{D}\mathbf{b}] \exp[-i\mathbf{k}(\mathbf{b}_+ - \mathbf{b}_-) - i\boldsymbol{\Delta}(z\mathbf{b}_+ + (1-z)\mathbf{b}_-)] = d^2\mathbf{b}d^2\mathbf{r} \exp[-i\boldsymbol{\Delta}\mathbf{b}] \exp[-i\mathbf{k}\mathbf{r}] , \tag{14}$$

so that

$$\begin{aligned}
\mathcal{A}_D(g^a N \rightarrow Q\bar{Q}N) &= \int d^2\mathbf{b}d^2\mathbf{r} \exp[-i\boldsymbol{\Delta}\mathbf{b}] \exp[-i\mathbf{k}\mathbf{r}] \psi_{\lambda,\bar{\lambda}}^{\lambda_g}(z, \mathbf{r}) \\
&\times \langle N | \mathcal{M}^a(\mathbf{b} + (1-z)\mathbf{r}, \mathbf{b} - z\mathbf{r}, \mathbf{b}) | N \rangle \\
&= t^a \int d^2\mathbf{b}d^2\mathbf{r} \exp[-i\boldsymbol{\Delta}\mathbf{b}] \exp[-i\mathbf{k}\mathbf{r}] \psi_{\lambda,\bar{\lambda}}^{\lambda_g}(z, \mathbf{r}) \\
&\times \left\{ \frac{1}{2N_c C_F} \Gamma^{(2)}(\mathbf{b} + (1-z)\mathbf{r}, \mathbf{b} - z\mathbf{r}) - \frac{N_c}{2C_F} \bar{\Gamma}^{(2)}(\mathbf{b} + (1-z)\mathbf{r}, \mathbf{b} - z\mathbf{r}) \right\} .
\end{aligned} \tag{15}$$

Now, the term  $\propto \bar{\Gamma}^{(2)}$  vanishes in the forward direction  $\boldsymbol{\Delta} = 0$ . For the forward amplitude we can then easily derive:

$$\begin{aligned}
\mathcal{A}_D(g^a N \rightarrow Q\bar{Q}N)|_{\boldsymbol{\Delta}=0} &= \frac{t^a}{2N_c C_F} \frac{4\pi}{N_c} \\
&\times \int \frac{d^2\boldsymbol{\kappa}}{\boldsymbol{\kappa}^4} \alpha_S \mathcal{F}(x_{\text{eff}}, \boldsymbol{\kappa}, -\boldsymbol{\kappa}) \left[ \psi_{\lambda,\bar{\lambda}}^{\lambda_g}(z, \mathbf{k}) - \psi_{\lambda,\bar{\lambda}}^{\lambda_g}(z, \mathbf{k} + \boldsymbol{\kappa}) \right] .
\end{aligned} \tag{16}$$

Here we have introduced the argument  $x_{\text{eff}}$  of the unintegrated gluon distribution, for which we take:

$$x_{\text{eff}} = x_{\mathbf{P}} = \frac{M^2}{\hat{s}} , \text{ with } M^2 = \frac{\mathbf{k}^2 + m_Q^2}{z(1-z)} . \tag{17}$$

As a matter of principle we should use an unintegrated gluon distribution which is also off-diagonal in the longitudinal momentum fractions of gluons. Here we neglect the effects of ‘‘skewedness’’, which could be expected to enhance the cross section. Remember

that in the hadron-level cross section there has a large uncertainty regarding the gap survival probability. In this view, we believe that our neglect of skewedness, and educated guessing of the slope, is justified. Furthermore various ratios shown in the results section should not be overly sensitive to these somewhat crude approximations.

Our amplitude can now be expressed in terms of the integrals that are found in [21]:

$$\left. \begin{matrix} \Phi_1 \\ \Phi_0 \end{matrix} \right\} = \int_0^\infty \frac{d\kappa^2}{\kappa^4} \alpha_S \mathcal{F}(x_{\text{eff}}, \boldsymbol{\kappa}, -\boldsymbol{\kappa}) \left\{ \begin{matrix} \frac{\mathbf{k}}{\mathbf{k}^2 + m_Q^2} W_1(\mathbf{k}^2, \boldsymbol{\kappa}^2, m_Q^2) \\ 1 \\ \frac{1}{\mathbf{k}^2 + m_Q^2} W_0(\mathbf{k}^2, \boldsymbol{\kappa}^2, m_Q^2), \end{matrix} \right. \quad (18)$$

$$W_1(\mathbf{k}, \boldsymbol{\kappa}^2, m_Q^2) = 1 - \theta(\mathbf{k}^2, \boldsymbol{\kappa}^2, m_Q^2), \quad (19)$$

$$W_0(\mathbf{k}, \boldsymbol{\kappa}^2, m_Q^2) = 1 - \frac{\mathbf{k}^2 + m_Q^2}{\sqrt{(\mathbf{k}^2 - m_Q^2 - \boldsymbol{\kappa}^2)^2 + 4\mathbf{k}^2 m_Q^2}}, \quad (20)$$

and

$$\theta(\mathbf{k}^2, \boldsymbol{\kappa}^2, m_Q^2) = \frac{\mathbf{k}^2 + m_Q^2}{2\mathbf{k}^2} \left( 1 + \frac{\mathbf{k}^2 - m_Q^2 - \boldsymbol{\kappa}^2}{\sqrt{(\mathbf{k}^2 - m_Q^2 - \boldsymbol{\kappa}^2)^2 + 4\mathbf{k}^2 m_Q^2}} \right). \quad (21)$$

Let us write out the amplitude explicitly for the different helicities (see e.g Eq.(108) in [19], here  $\mathbf{e}(\lambda_g) = -(\lambda_g \mathbf{e}_x + i \mathbf{e}_y)/\sqrt{2}$ ):

$$\begin{aligned} \mathcal{A}_D(g_{\lambda_g}^a N \rightarrow Q_\lambda \bar{Q}_{\bar{\lambda}} N) |_{\Delta=0} &= \frac{t^a}{2N_c C_F} \frac{4\pi^2}{N_c} \sqrt{\alpha_S} \\ &\left\{ 2\delta_{\lambda-\bar{\lambda}} \left[ z\delta_{\lambda_g\lambda} - (1-z)\delta_{\lambda_g\bar{\lambda}} \right] (\Phi_1 \cdot \mathbf{e}(\lambda_g)) \right. \\ &\left. - \delta_{\lambda\bar{\lambda}} \delta_{\lambda_g\lambda} \sqrt{2} m_Q \Phi_0 \right\} \end{aligned} \quad (22)$$

Then, if we put everything together, we get for the differential parton-level cross section.

$$16\pi \frac{d\hat{\sigma}(gN \rightarrow Q\bar{Q}N; \hat{s})}{dz d^2\mathbf{k} d\Delta^2} \Big|_{\Delta^2=0} = \frac{1}{2 \cdot (N_c^2 - 1)} \cdot \sum_{\lambda_g, \lambda, \bar{\lambda}, a} \left| \mathcal{A}_D(g_{\lambda_g}^a N \rightarrow Q_\lambda \bar{Q}_{\bar{\lambda}} N) \right|^2 dz \frac{d^2\mathbf{k}}{(2\pi)^2}, \quad (23)$$

and the final multi-dimensional cross section reads:

$$\frac{d\hat{\sigma}(gN \rightarrow Q\bar{Q}N; \hat{s})}{dz d^2\mathbf{k} d\Delta^2} \Big|_{\Delta^2=0} = \frac{\pi}{4 N_c^2 (N_c^2 - 1)^2} \alpha_S \left\{ [z^2 + (1-z)^2] \Phi_1^2 + m_Q^2 \Phi_0^2 \right\}. \quad (24)$$

### A. Hard scale, quark-mass dependence and twist-expansion

In order to expose the dependence on the heavy quark mass  $m_Q$ , and/or the hard scale of the process  $\bar{Q}^2 = \mathbf{k}^2 + m_Q^2$ , it is useful to develop the twist expansion of the diffractive amplitude and extract the piece leading in  $\bar{Q}^2$ .

The starting point would be an expansion of weight functions  $W_{0,1}$  in powers of  $\kappa^2/\bar{Q}^2$ . From the Taylor expansion

$$\frac{1}{\sqrt{(\mathbf{k}^2 - m_Q^2 - \kappa^2)^2 + 4\mathbf{k}^2 m_Q^2}} = \frac{1}{\bar{Q}^2} \left( 1 + \kappa^2 \frac{\mathbf{k}^2 - m_Q^2}{\bar{Q}^4} + \dots \right), \quad (25)$$

we obtain

$$W_1(\mathbf{k}, \kappa^2, m_Q^2) \simeq \frac{2m_Q^2}{[\mathbf{k}^2 + m_Q^2]^2} \cdot \kappa^2, \quad W_0(\mathbf{k}, \kappa^2, m_Q^2) \simeq \frac{\mathbf{k}^2 - m_Q^2}{[\mathbf{k}^2 + m_Q^2]^2} \cdot \kappa^2. \quad (26)$$

As it must be, the weight functions for small  $\kappa^2$  vanish  $\propto \kappa^2$ , so that we obtain a large contribution to the diffractive amplitude which is proportional to the integrated gluon distribution  $xg(x, \bar{Q}^2)$ :

$$\int^{\bar{Q}^2} \frac{d\kappa^2}{\kappa^4} \cdot \kappa^2 \cdot \alpha_S \frac{\partial[xg(x, \kappa^2)]}{\partial \log(\kappa^2)} = \alpha_S(\bar{Q}^2) xg(x, \bar{Q}^2), \quad (27)$$

where  $\bar{Q}^2 = \mathbf{k}^2 + m_Q^2$ . This is the ‘‘leading twist’’ contribution in which virtualities  $\kappa^2$  of exchanged gluons are much smaller than the virtualities of the quark lines, and thus we can integrate out the gluon transverse momenta. Introducing  $\tau \equiv \mathbf{k}^2/m_Q^2$ , we find for the differential cross section (24) the result

$$\left. \frac{d\hat{\sigma}(gN \rightarrow Q\bar{Q}N; \hat{s})}{dzd\tau d\Delta^2} \right|_{\Delta^2=0} = \frac{\pi^2}{4N_c^2(N_c^2 - 1)^2 m_Q^4} \frac{1}{(1 + \tau)^6} \frac{(1 - \tau)^2 + [z^2 + (1 - z)^2]4\tau}{1} \times \alpha_S^3((1 + \tau)m_Q^2) \left[ x_{\text{eff}} g(x_{\text{eff}}, (1 + \tau)m_Q^2) \right]^2. \quad (28)$$

Here the scaling of the cross section with  $m_Q^{-4}$  is put in evidence. It is only violated by the argument of the running coupling and the integrated gluon of the target. We notice that this approximation is used throughout in earlier works on charm production in deep inelastic and hadronic reactions [14–16].

We note parenthetically, that the leading twist approximation is expected to work well for  $\tau \lesssim 1$  and for the integrated cross section. It will be inadequate for jet production, at large jet transverse momenta  $\tau \gg 1$ . In this case the weight functions  $W_{0,1}$  will develop sharp peaks at around  $\kappa^2 \sim \mathbf{k}^2$ , the twist expansion breaks down, and the diffractive amplitude will then be dominated by a piece that is directly proportional to the unintegrated gluon distribution of the proton [22].

We go beyond the approximation (28), and in our numerical calculations always use the  $\mathbf{k}_\perp$ -factorization representation (24).

Finally a comment on earlier works is in order. Alves et al. [15] replace in the diagrams of Fig.2 the incoming gluon by an effective color singlet current, and hence have no diagram in which the two  $t$ -channel gluons couple to the incoming gluon. While this gives the correct structure of the amplitude, the correct normalization can only be found by doing the proper color algebra in the full set of diagrams. Furthermore, Alves et al. [15] also consider diagrams of the type shown in Fig.3. Notice that when the two



$t$ -channel gluons are coupled to the proton, each of these diagrams has two cuts which contribute to the imaginary part of the amplitude, one in which the  $s$ -channel gluon line is cut, and another one where the (anti-)quark line is cut. In the high energy limit of  $M_{Q\bar{Q}}^2/\hat{s} \ll 1$  these two contributions cancel each other. This is a technical manifestation of an ‘‘LPM’’-like phenomenon: in the limit of large coherence length, the radiation between scatterings vanishes (for a review of LPM-physics in perturbative QCD, see e.g. [23]). In Ref.[15] the diagrams of Fig.3 give the dominant contribution, but it appears that only the cut through the gluon line has been accounted for, and the cut through the (anti-)quark line apparently has been overlooked.

The authors of Ref.[16] state, that the diagrams of Fig.3 are necessary to cancel soft divergences – this is not borne out by our calculation, our final results also differ from those in [16].

## B. Hadron-level cross section

We finally want to calculate for example the spectrum of quarks in the  $pp$ -collision. Starting from the diffractive  $gp \rightarrow Q\bar{Q}p$  cross section

$$\left. \frac{d\hat{\sigma}(gN \rightarrow Q\bar{Q}N; \hat{s})}{dzd^2\mathbf{k}d\Delta^2} \right|_{\Delta^2=0} = \hat{f}_{Q\bar{Q}}(z, \mathbf{k}; \hat{s}) \quad (29)$$

we can obtain the corresponding cross section for  $pp$ -collisions in the collinear approximation for the incoming gluon as:

$$\begin{aligned} \left. \frac{d\sigma(pp \rightarrow XQ\bar{Q} + p; s)}{dx_Q d^2\mathbf{k}d\Delta^2} \right|_{\Delta^2=0} &= \int dx dz \delta(x_Q - xz) g(x, \bar{Q}^2) \hat{f}_{Q\bar{Q}}(z, \mathbf{k}; xs) , \\ &= \int_{x_Q}^1 \frac{dx}{x} g(x, \bar{Q}^2) \hat{f}_{Q\bar{Q}}\left(\frac{x_Q}{x}, \mathbf{k}; xs\right). \end{aligned} \quad (30)$$

We can also calculate the fully differential distribution in  $x_Q, x_{\bar{Q}} = x - x_Q$ , rapidities etc.

$$\left. \frac{d\sigma(pp \rightarrow XQ\bar{Q} + p; s)}{dx_Q dx_{\bar{Q}} d^2\mathbf{k}d\Delta^2} \right|_{\Delta^2=0} = \frac{1}{x_Q + x_{\bar{Q}}} g(x_Q + x_{\bar{Q}}, \bar{Q}^2) \hat{f}_{Q\bar{Q}}\left(\frac{x_Q}{x_Q + x_{\bar{Q}}}, \mathbf{k}; xs\right). \quad (31)$$

Alternatively, the rapidity distributions of quarks may be of interest. Let the incoming protons have the four momenta

$$p_A = \sqrt{\frac{s}{2}}n_+ + \frac{m_p^2}{2}\sqrt{\frac{2}{s}}n_-, \quad p_B = \frac{m_p^2}{2}\sqrt{\frac{2}{s}}n_+ + \sqrt{\frac{s}{2}}n_-, \quad (32)$$

with

$$n_{\pm} = \frac{1}{\sqrt{2}}(1, 0, 0, \pm 1), \quad p_A^2 = p_B^2 = m_p^2, \quad 2p_A p_B = s + \mathcal{O}\left(\frac{m^4}{s}\right). \quad (33)$$

The four-momenta of quark and antiquark are then

$$\begin{aligned} p_Q &= x_Q p_A^+ n_+ + \frac{\mathbf{k}^2 + m_Q^2}{2x_Q p_A^+} n_- + k_\perp, \\ p_{\bar{Q}} &= x_{\bar{Q}} p_A^+ n_+ + \frac{\mathbf{k}^2 + m_Q^2}{2x_{\bar{Q}} p_A^+} n_- - k_\perp. \end{aligned} \quad (34)$$

Instead of  $x_Q, x_{\bar{Q}}$  one often uses the rapidities:

$$y_Q = \frac{1}{2} \log \left( \frac{p_Q^+}{p_Q^-} \right), \quad y_{\bar{Q}} = \frac{1}{2} \log \left( \frac{p_{\bar{Q}}^+}{p_{\bar{Q}}^-} \right). \quad (35)$$

Explicitly:

$$y_Q = \log \left( \frac{x_Q \sqrt{s}}{\sqrt{\mathbf{k}^2 + m_Q^2}} \right), \quad y_{\bar{Q}} = \log \left( \frac{x_{\bar{Q}} \sqrt{s}}{\sqrt{\mathbf{k}^2 + m_Q^2}} \right). \quad (36)$$

The rapidity difference  $\Delta y$ , and average rapidity  $Y = (y_Q + y_{\bar{Q}})/2$  of quark and antiquark are

$$\begin{aligned} \Delta y &= y_Q - y_{\bar{Q}} = \log \left( \frac{x_Q}{x_{\bar{Q}}} \right) = \log \left( \frac{z}{1-z} \right), \\ Y &= \frac{1}{2}(y_Q + y_{\bar{Q}}) = \frac{1}{2} \log \left( \frac{x_Q x_{\bar{Q}} s}{\mathbf{k}^2 + m_Q^2} \right) = \frac{1}{2} \log \left( \frac{x}{x_{\mathbf{P}}} \right). \end{aligned} \quad (37)$$

Notice that the dissociating proton is at positive rapidity. In fact  $y_A = \log(\sqrt{s}/m_p) \sim +9.5$ , while  $y_B = \log(m_p/\sqrt{s}) \sim -9.5$  at the nominal LHC energy.

### III. NUMERICAL RESULTS

In our numerical calculations, we shall use three different unintegrated gluon distribution functions (UGDFs) from the literature. One of them from Ref.[24] (labelled Ivanov-Nikolaev) is a fit to HERA structure functions data. The other two, from Ref.[25] (labelled Kutak-Stasto) are obtained by solving a BFKL equation accounting for subleading terms. One of the latter UGDFs also accounts for a nonlinear Balitsky-Kovchegov type term in the evolution equation. Both UGDF sets give a reasonable description of deep inelastic structure functions at small  $x$ .

For the argument of running coupling constant we take:  $\mu_r^2 = M_{Q\bar{Q}}^2$  for  $g \rightarrow Q\bar{Q}$  splitting and  $\mu^2 = \max(\kappa^2, \mathbf{k}^2 + m_Q^2)$  for the  $t$ -channel coupling of gluons to heavy quarks. For the quark masses, we take  $m_c = 1.5$  GeV and  $m_b = 4.75$  GeV

Before we shall show differential distributions let us discuss integrated cross section for single diffractive process for  $Q\bar{Q}$  production. In Table I we have collected the integrated cross section for different UGDFs and different GDFs from the literature [26–28]. Here we have not included a gap survival factor. The cross section for  $b\bar{b}$  is about two orders

TABLE I: Integrated cross section in mb for single diffractive production of  $c\bar{c}$  and  $b\bar{b}$  for different UGDFs and GDFs at  $\sqrt{s} = 14$  TeV. No gap survival factor was included here.

UGDF	GDF	$\sigma(c\bar{c})$ [mb]	$\sigma(b\bar{b})$ [mb]	$\sigma(b\bar{b})/\sigma(c\bar{c})$
IN	GRV94	1.3891 e-2	1.4201 e-4	1 %
	GJR08	1.0954 e-2	1.1083 e-4	1 %
	CTEQ6	1.7607 e-2	1.3808 e-4	0.7 %
KS (lin.)	GRV94	1.4837 e-2	1.0293 e-4	0.7 %
	GJR08	1.0402 e-2	0.9011 e-4	0.9 %
	CTEQ6	1.9719 e-2	1.0789 e-4	0.5 %
KS (non lin.)	GRV94	1.0122 e-2	0.9185 e-4	0.9 %
	GJR08	0.8322 e-2	0.9005 e-4	1 %
	CTEQ6	1.2335 e-2	0.9311 e-4	0.8 %

of magnitude smaller than that for  $c\bar{c}$ , which is well in line with the expected  $m_Q^{-4}$  scaling:  $(m_c/m_b)^4 \sim 1\%$ . We observe a dependence of the cross section on the choice of UGDF, especially for  $c\bar{c}$  production. Particularly interesting is the difference between results with linear and nonlinear versions of the Kutak-Stašto UGDF. The difference between different UGDFs points to the fact that single diffractive production of charm tests UGDFs in the region of very small  $x_{\mathbf{P}}$ . We shall return to the impact of UGDFs on differential distributions somewhat later in this section. The dependence of the cross section on the choice of different GDFs is of a similar size. Again the largest differences are observed for charm production, which is expected as the small- $x$  glue is probed at somewhat smallish hard scales.

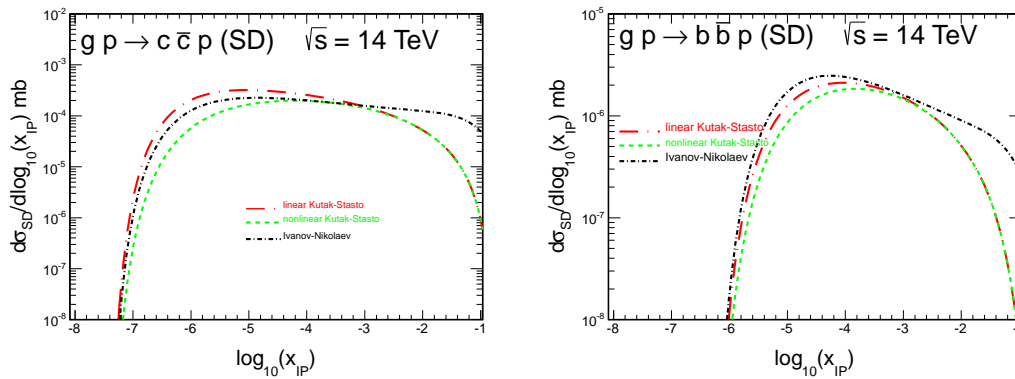


FIG. 4: Distribution in  $\log_{10}(x_{\mathbf{P}})$  for  $c\bar{c}$  (left) and  $b\bar{b}$  (right) produced in a single diffractive process for center of mass energy  $\sqrt{s} = 14$  TeV for the Ivanov-Nikolaev (solid), linear Kutak-Stašto (dashed) and nonlinear Kutak-Stašto (dotted) UGDFs. Absorptive effects have been included by multiplying by gap survival factor.

Now we wish to present differential distributions. Here, absorption corrections are included in a rough manner, by multiplying the cross section by a gap survival factor  $S_G = 0.05$  [4, 5]. A more subtle treatment, which would include the dependence of

absorption effects on kinematical variables goes beyond the scope of the present work, but must be developed in the future.

Let us start with distributions in  $x_{\mathbf{P}}$  – the fractional longitudinal momentum loss of proton. Notice that  $\log(1/x_{\mathbf{P}})$  is proportional to the size of the rapidity gap. The cross section drops sharply at  $x_{\mathbf{P}} \lesssim 10^{-7}$  for charm quarks and  $x_{\mathbf{P}} \lesssim 10^{-6}$  for bottom quarks. This is related to the fact that with increasing gap size we are asking for harder partons in the dissociating proton. The gluon distribution however drops sharply at large  $x$ .

Notice, that in the Ingelman-Schlein model, the gap size-dependence is described in terms of a universal flux of Pomerons. In our microscopic model the  $x_{\mathbf{P}}$ -dependence is driven by the dependence of the unintegrated gluon distribution on  $x_{\text{eff}} = x_{\mathbf{P}}$ .

We observe a breaking of Regge factorization: the gap-size dependence is substantially steeper for bottom production than for charm production. It reminds us of the systematics of the energy dependence of diffractive photo/leptoproduction of vector mesons as well as inclusive deep inelastic diffraction, where also a dependence of the effective Pomeron intercept on the relevant hard scale is observed. In Fig.5 we show a distribu-

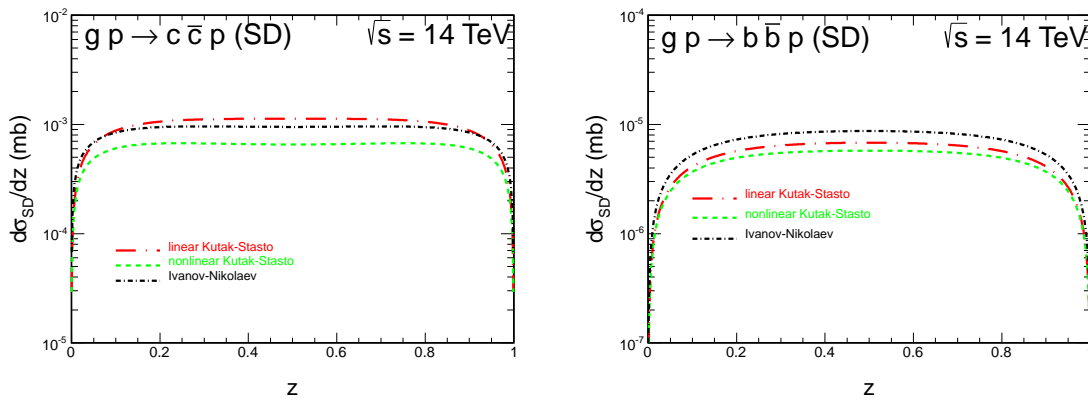


FIG. 5: Distribution in  $z$  of  $c$  ( $\bar{c}$ ) (left) and  $b$  ( $\bar{b}$ ) (right) produced in a single diffractive process for center of mass energy  $\sqrt{s} = 14$  TeV for the Ivanov-Nikolaev and the Kutak-Stašto UGDFs. Absorptive effects have been included by multiplying the model cross section by gap survival factor.

tion in longitudinal momentum fraction of quark with respect to the parent gluon. It is fairly uneventful and simply reflects the  $z$ -dependence in evidence in Eq.(24). The distribution is broad, it vanishes at the endpoints, because there the invariant mass of the  $Q\bar{Q}$  system becomes large, and the unintegrated gluon distribution drops steeply at  $x_{\text{eff}} \rightarrow 1$ .

In Fig.6 we present the rapidity distribution of charm (left panel) and bottom (right panel) quarks/antiquarks from diagram (b) in Fig.1. At large rapidities the cross section with the Ivanov-Nikolaev UGDF is much larger than that with the nonlinear Kutak-Stašto UGDF. This is partially due to nonlinear effects included in the latter distributions. The nonlinear effects show up at  $x_{\mathbf{P}} < 10^{-4}$ .

In Fig.7 we show transverse momentum distributions of charm (left panel) and bottom (right panel) quarks/antiquarks from one single-diffractive mechanism. The spread in

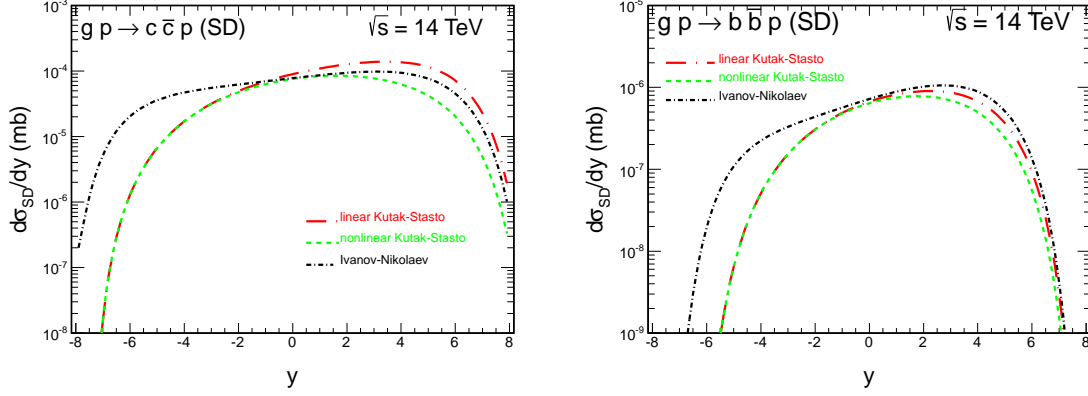


FIG. 6: Distribution in rapidity of  $c$  ( $\bar{c}$ ) (left) and  $b$  ( $\bar{b}$ ) (right) produced in a single diffractive process for center of mass energy  $\sqrt{s} = 14$  TeV. Absorptive effects have been included by multiplying by gap survival factor.

transverse momentum here is somewhat smaller than in the Ingelman-Schlein model calculations of Ref.[9]. Finally in Fig.8 we show distribution in the quark-antiquark

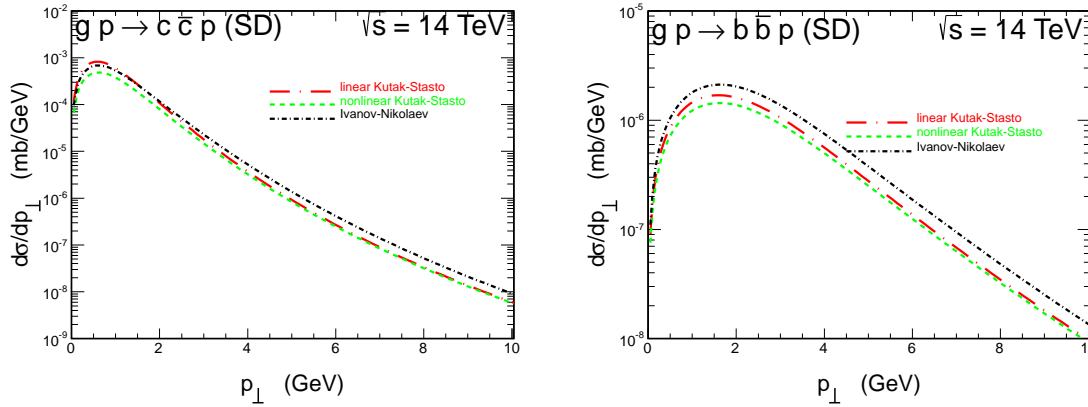


FIG. 7: Distribution in transverse momentum of  $c$  ( $\bar{c}$ ) (left) and  $b$  ( $\bar{b}$ ) (right) produced in a single diffractive process for center-of-mass energy  $\sqrt{s} = 14$  TeV. Absorptive effects have been included by multiplying by gap survival factor.

invariant mass. Rather low invariant masses (small rapidity difference between quark and antiquark) close to the  $Q\bar{Q}$  threshold, especially for  $c\bar{c}$  production, are populated.

Now we wish to study dependence of the ratio of cross sections for  $b\bar{b}$  and  $c\bar{c}$  production as a function of several kinematical variables, which should be to a good approximation independent of absorption. In Fig.9 we show the ratio as a function of quark rapidity. The ratio for the Ingelman-Schlein model is somewhat larger than that for the gluon-dissociation approach. The charm-to-bottom ratio as a function of transverse momentum of the (anti)quark is shown in Fig.10. The ratio increases as a function of quark transverse momentum. The character of the function is in principle similar for both models. In

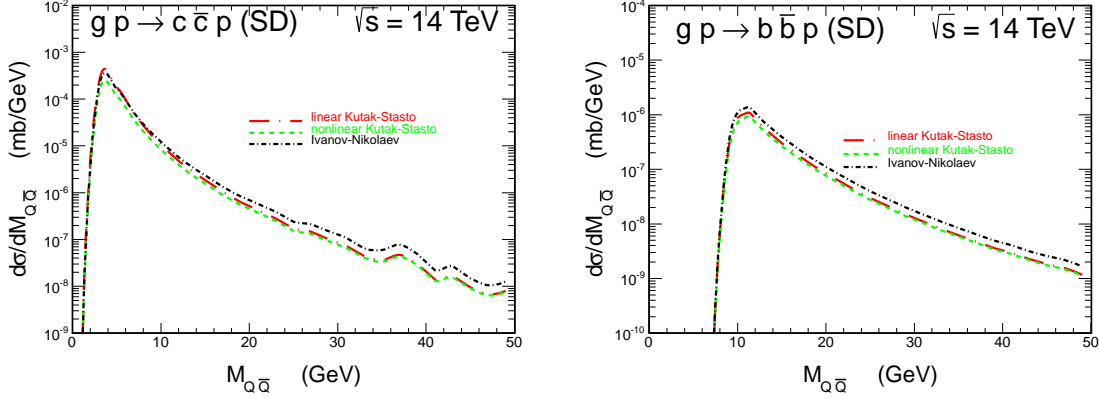


FIG. 8: Distribution in invariant mass of  $c\bar{c}$  (left) and  $b\bar{b}$  (right) system produced in a single diffractive process for center of mass energy  $\sqrt{s} = 14$  TeV. Absorptive effects have been included by multiplying by gap survival factor.

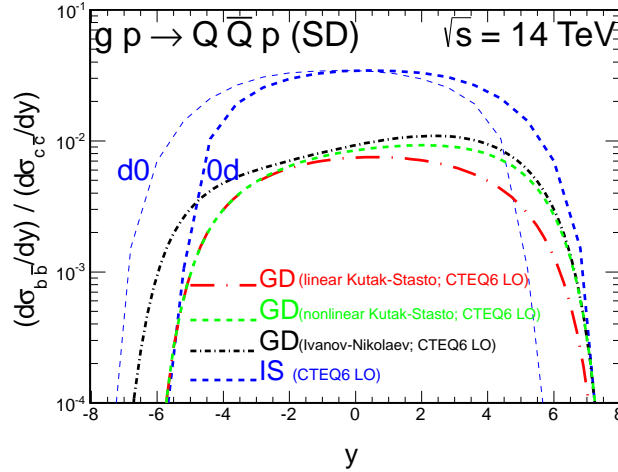


FIG. 9: The ratio of the  $b\bar{b}$  to  $c\bar{c}$  distributions in quark (antiquark) rapidity.

Fig.11 we show similar ratio as a function of  $\log_{10}x_{\mathbf{P}}$ . Here we see that the gluon dissociation mechanism and the Ingelman-Schlein model exhibit an opposite trend with increasing gap size: the  $b\bar{b}$  fraction increases for the gluon dissociation model and decreases for the Ingelman-Schlein case. Finally, in Fig.12 we show the ratio as a function of diffractively produced mass  $M_X$ . The dependences for both models are rather smooth.

#### IV. CONCLUSIONS AND OUTLOOK

In the present paper we have discussed forward amplitudes for the  $gp \rightarrow Q\bar{Q}p$  subprocess both in the impact parameter and momentum space representation in the for-

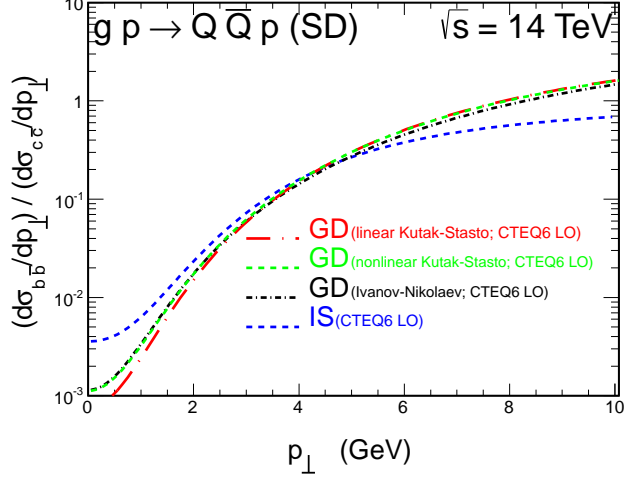


FIG. 10: The ratio of the  $b\bar{b}$  to  $c\bar{c}$  distributions in quark (antiquark) transverse momentum.

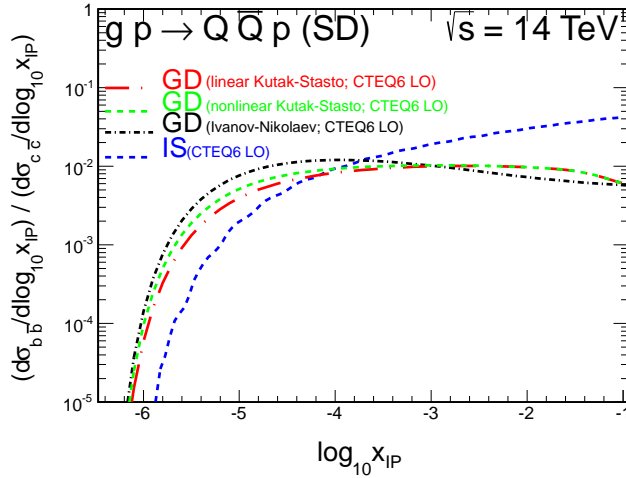


FIG. 11: The ratio of the  $b\bar{b}$  to  $c\bar{c}$  distributions in  $\log_{10}(x_{\mathbf{P}})$ .

ward scattering approximation. The amplitude for the off-forward directions within the diffraction cone was extrapolated by assuming exponential dependence known from other diffractive processes. The forward amplitude for the  $gp \rightarrow Q\bar{Q}p$  subprocess has been obtained in terms of unintegrated gluon distribution of the target proton.

The formulae have been used to calculate cross section for the single scattering process  $pp \rightarrow Q\bar{Q}pX$  as a convolution of the collinear gluon distributions in the proton and the elementary  $gp \rightarrow Q\bar{Q}p$  cross section both for charm and bottom production. When applied to the hadronic collisions, this approach allows one to predict heavy quark production “close to the gap”. In other words the heavy quarks are produced in the Pomeron fragmentation region.

Three different unintegrated gluon distributions describing deep-inelastic data at

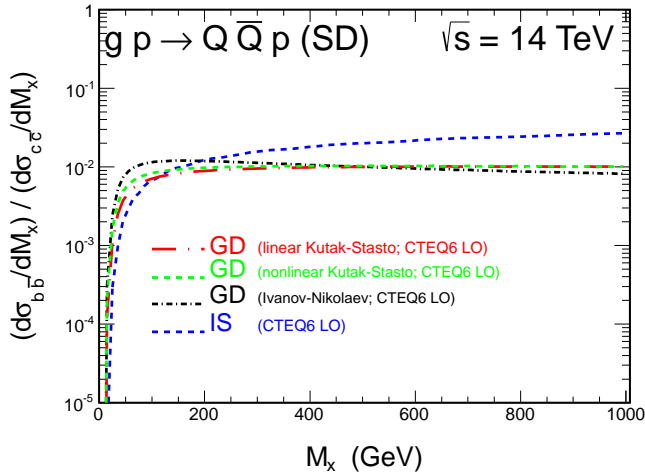


FIG. 12: The ratio of the  $b\bar{b}$  to  $c\bar{c}$  distributions in  $M_X$ .

HERA, known from the literature, have been used.

We have presented first results for the rapidity and transverse momentum distribution of quarks (antiquarks) and  $Q\bar{Q}$  invariant mass at the nominal LHC energy  $\sqrt{s} = 14$  TeV. The cross section for charm quarks is two orders of magnitude larger than that for bottom quarks, as expected from the  $m_Q^{-4}$  scaling of the partonic subprocess.

We have calculated also ratio of the cross section for  $b\bar{b}$  and  $c\bar{c}$  as a function of several kinematical variables. The ratio is fairly smooth in (anti)quark rapidity and strongly depends on (anti)quark transverse momentum.

It would be interesting to extend the present microscopic model to higher Fock-states, like  $Q\bar{Q}g$ . This would make it possible to also discuss heavy quark production “far away from the gap”, which up to now is modelled in the Ingelman-Schlein approach. We believe that a more microscopic approach may make it possible to find sources of Regge factorization breaking, and perhaps to ultimately include absorption effects on an equal footing.

A measurement of the single diffractive production would be possible e.g. at ATLAS detector by using so-called ALFA detectors for measuring forward protons and their fractional energy loss and the main central detector for the measurement of  $D$  or  $B$  mesons. CMS+TOTEM is another option. Further evaluation of the cross section including  $c \rightarrow D$  or  $b \rightarrow B$  fragmentation and experimental cuts on pseudorapidities and transverse momenta of  $D$  mesons and protons) would be very useful in planning and performing measurements. Such measurements should be possible after the technical shut down in 2013-2014.

### Acknowledgment

This work was partially supported by the Polish MNiSW grant DEC-



- 
- [1] M. Boonekamp, F. Chevallier, C. Royon and L. Schoeffel, *Acta Phys. Polon. B* **40** (2009) 2239 [arXiv:0902.1678 [hep-ph]].
  - [2] G. Ingelman and P. E. Schlein, *Phys. Lett. B* **152**, 256 (1985).
  - [3] J. D. Bjorken, *Phys. Rev. D* **47** (1993) 101.
  - [4] V. A. Khoze, A. D. Martin and M. G. Ryskin, *Eur. Phys. J. C* **18**, 167 (2000) [arXiv:hep-ph/0007359].
  - [5] U. Maor, *AIP Conf. Proc.* **1105**, 248 (2009) [arXiv:0811.2636 [hep-ph]].
  - [6] H. Fritzsche and K. H. Streng, *Phys. Lett. B* **164**, 391 (1985).
  - [7] M. Heyssler, *Z. Phys.* **C73** (1997) 299
  - [8] M.B. Gay Ducati, M.M. Machado and M.V.T Machado, *Phys. Rev.* **D81** (2010) 054034.
  - [9] M. Łuszczak, R. Maciula and A. Szczurek, *Phys. Rev.* **D84** (2011) 114018.
  - [10] N. Nikolaev and B. G. Zakharov, *Z. Phys. C* **53**, 331 (1992).
  - [11] M. Genovese, N. N. Nikolaev and B. G. Zakharov, *J. Exp. Theor. Phys.* **81** (1995) 625 [*Zh. Eksp. Teor. Fiz.* **108** (1995) 1141] [hep-ph/9410273].
  - [12] J. Bartels, J. R. Ellis, H. Kowalski and M. Wüsthoff, *Eur. Phys. J. C* **7** (1999) 443 [hep-ph/9803497].
  - [13] N. N. Nikolaev, W. Schäfer, B. G. Zakharov and V. R. Zoller, *JETP Lett.* **80** (2004) 371 [*Pisma Zh. Eksp. Teor. Fiz.* **80** (2004) 423] [hep-ph/0408113].
  - [14] M. Genovese, N. N. Nikolaev and B. G. Zakharov, *Phys. Lett. B* **378**, 347 (1996) [hep-ph/9603285].
  - [15] G. Alves, E. Levin and A. Santoro, *Phys. Rev. D* **55**, 2683 (1997) [hep-ph/9608443].
  - [16] F. Yuan and K. -T. Chao, *Phys. Rev. D* **60**, 094012 (1999) [hep-ph/9810340].
  - [17] B. Z. Kopeliovich, I. K. Potashnikova, I. Schmidt and A. V. Tarasov, *Phys. Rev. D* **76**, 034019 (2007) [hep-ph/0702106 [HEP-PH]].
  - [18] N. N. Nikolaev and W. Schäfer, *Phys. Rev. D* **71**, 014023 (2005) [hep-ph/0411365].
  - [19] I. P. Ivanov, N. N. Nikolaev and A. A. Savin, *Phys. Part. Nucl.* **37** (2006) 1 [hep-ph/0501034].
  - [20] I. P. Ivanov, N. N. Nikolaev and W. Schäfer, *Phys. Part. Nucl.* **35** (2004) S30.
  - [21] N. N. Nikolaev, A. V. Pronyaev and B. G. Zakharov, *Phys. Rev. D* **59**, 091501 (1999) [hep-ph/9812212].
  - [22] N. N. Nikolaev and B. G. Zakharov, *Phys. Lett. B* **332**, 177 (1994) [hep-ph/9403281].
  - [23] R. Baier, D. Schiff and B. G. Zakharov, *Ann. Rev. Nucl. Part. Sci.* **50** (2000) 37 [hep-ph/0002198].
  - [24] I. Ivanov and N.N. Nikolaev, *Phys. Rev.* **D65** (2002) 054004.
  - [25] K. Kutak and A. Staśto, *Eur. Phys. J.* **C41** (2005) 343.
  - [26] M. Glück, E. Reya and A. Vogt, *Z. Phys.* **C67** (1995) 433.
  - [27] J. Pumplin, D.R. Stump, J. Huston, H.L. Lai, P.M. Nadolsky and W.K. Tung, *JHEP*0207 (2002) 012.
  - [28] M. Glück, D. Jimenez-Delgado and E. Reya, *Eur. Phys. J.* **C53** (2008) 355;  
M. Glück, D. Jimenez-Delgado, E. Reya and C. Schuck, *Phys. Lett.* **B664** (2008) 133.

